



**HAL**  
open science

# Fabrication of 3D microdevices from planar electroplating for the isolation of cancer associated cells in blood

Elise Bou, Alejandro Kayum Jimenez Zenteno, Aurore Estève, David Bourrier, Christophe Vieu, Aline Cerf

► **To cite this version:**

Elise Bou, Alejandro Kayum Jimenez Zenteno, Aurore Estève, David Bourrier, Christophe Vieu, et al.. Fabrication of 3D microdevices from planar electroplating for the isolation of cancer associated cells in blood. *Microelectronic Engineering*, 2019, 213, pp.69-76. 10.1016/j.mee.2019.04.010 . hal-02336950

**HAL Id: hal-02336950**

**<https://laas.hal.science/hal-02336950>**

Submitted on 29 Oct 2019

**HAL** is a multi-disciplinary open access archive for the deposit and dissemination of scientific research documents, whether they are published or not. The documents may come from teaching and research institutions in France or abroad, or from public or private research centers.

L'archive ouverte pluridisciplinaire **HAL**, est destinée au dépôt et à la diffusion de documents scientifiques de niveau recherche, publiés ou non, émanant des établissements d'enseignement et de recherche français ou étrangers, des laboratoires publics ou privés.

# Fabrication of 3D microdevices from planar electroplating for the isolation of cancer associated cells in blood

Elise Bou<sup>a, b</sup>, Alejandro K. Jiménez-Zenteno<sup>a</sup>, Aurore Estève<sup>a</sup>, David Bourrier<sup>a</sup>, Christophe Vieu<sup>a</sup>, Aline Cerf<sup>a, \*</sup>

<sup>a</sup> LAAS-CNRS, Université de Toulouse, CNRS, INSA, UPS, 7 Avenue du Colonel Roche, 31400 Toulouse, France

<sup>b</sup> SmartCatch, 1 Avenue Irène Joliot-Curie, 31100 Toulouse, France

\*Corresponding author. Email address: [acerf@laas.fr](mailto:acerf@laas.fr)

## Abstract

Malignant cells detaching from a primary tumor to reach the bloodstream are known as circulating tumor cells (CTCs). Enumeration and molecular characterizations of these cells have been used as prognostic cancer biomarkers. Various *in vitro* techniques are available to extract these biomarkers from blood samples, although their performances are limited by the amount of blood available for analysis, usually 7.5 mL, and the rareness of these cells as a few per mL. To address this sampling bias we propose a three-dimensional (3D) microdevice adapted to the *in vivo* isolation of CTCs in the venous blood flow. Our device acts as an *in vivo* microfilter in which CTCs are specifically retained due to their specific morphological and mechanical properties as compared to normal blood cells. We present the fabrication process of these devices using planar silicon technology and their adaptation to generate a 3D microfilter integrated into a compatible medical consumable for venous access. We demonstrate that these devices are capable to capture human prostate cancer cells (PC3) spiked into whole blood using a fluidic platform mimicking an artificial vein. Moreover, the captured cells can be easily characterized by conventional microscopy and readily available for functional and downstream analysis. This minimally invasive technology could offer high-quality information to physicians and serve as a tool for personalized therapeutic follow-up in clinical routine.

**Keywords :** Circulating Tumor Cells; microfiltration; medical device; 3D fabrication; electroplating

## 1. Introduction

Tissue analyses obtained by surgical intervention drives characterization and treatment of solid tumors. However, the sampling frequency is limited by the invasive access to the primary tumor or metastases and it is therefore difficult to obtain representative information to monitor cancer evolution. Direct access to the bloodstream and the cancer-associated biomarkers that it carries represents a potential alternative to solid biopsy in cancer care. Circulating tumor cells (CTCs) are tumor cells detaching from a solid tumor to access the bloodstream by means of a process known as EMT (Epithelial to Mesenchymal Transition). Presence of CTCs in blood is associated with increased tumor aggressiveness and metastatic risk. A correlation has been demonstrated between the number of CTCs per unit of blood volume and patient prognosis [1]. Extracting CTCs from blood and performing adequate functional analysis could provide phenotypic and genotypic information related to both primary and metastatic tumors [2]. Therefore, CTCs are the center of attention of various studies their potential use as biomarkers. Detection, isolation and analysis of CTCs are promising for cancer diagnosis and prognosis, as well as for the monitoring of treatment in cancer patients.

CTC population is extremely rare among different blood cell types. Typical concentration is estimated at one CTC for one billion of normal blood cells in patients with metastatic cancer, equivalent to a single cell in less than 1mL of blood, thus rendering their detection challenging. Current *in vitro* systems

for CTC isolation can be classified in two categories: immunoaffinity-based and physical properties-based technologies. The physical approach takes advantage of specific physical traits of CTCs, such as density, size, deformability and dielectrical properties [3]. Exploiting their larger size and increased stiffness of CTCs compared to normal blood cells [4], microfiltration systems represent a wide branch of CTC isolation techniques with several reported devices [5]. Those systems have the inconvenience of requiring long processing times and operating at relatively high-pressure conditions [6]. Immunoaffinity techniques use engineered antibodies directed against antigens expressed by CTCs. One of the most commonly used antibody targets the epithelial cell adhesion molecule (EpCAM) normally found in neoplastic epithelial cells. Based on this approach, different technologies have been proposed using functionalized magnetic beads, microfluidic channels, or nanostructured substrates [5]. Diverse *in vitro* devices have been developed based on these two approaches, however, these systems are limited by the volume of blood available, sampling frequency, sample preparation and sample processing. Using an *in vivo* approach could offer the advantages of screening higher volumes of blood, increasing the interrogation frequency, and performing cell isolation under physiological flow conditions favoring the preservation of cell viability. Up to now, only one *in vivo* method for CTC enrichment has been implemented based on the immunoaffinity approach consisting in a medical wire functionalized with EpCAM antibodies [7]. However, the expression of CTC membrane antigens can vary widely among different cancer types and among various CTCs originating from the same tumor. This heterogeneity causes a major limitation for the immunoaffinity approach which uses specific antigens not capable to target the entire population of malignant cells.

Here we propose an innovative intravascular device enabling the trapping of CTCs in human blood based solely on their physical characteristics. Using a filtration approach, we developed a fishnet-like three-dimensional (3D) microdevice integrated into a conventional medical catheter. The device exposed to the bloodstream could potentially enable the filtration of a relatively high volume of blood, thus considerably increasing the probability of detecting rare events. In addition, our devices were designed to facilitate the characterization of trapped cells.

## 2. Concept of 3D microfiltration

Several techniques for *ex vivo* microfiltration have been implemented resulting in a variety of devices using 2D filters to isolate CTCs based on size from blood samples. Based on this principle, some track-etched isopore membranes have been implemented for CTC enrichment and analysis such as ISET® [8] and work reported by *Ntouroupi et al.* [9]. Micropatterned membranes based on photolithography techniques allowing to control pore size, shape and distribution have also been proposed in a wide range of materials. An example of filtering membranes made of polymer such as SU-8 has been reported by *Adams et al.* [10]. The principle of cancer cell isolation implemented with our microdevices relies on a filter-based approach involving a 2.5D engineered microfilter. The microfilter consists in a hollow circular cylinder with a holey membrane at the downstream end-wall (Figure 1a). The holey membrane contains uniformly distributed circular pores acting as a filter physically retaining cells larger than the pore-size. Our capture microdevices were designed to be inserted into a superficial vein of the human forearm *via* a conventional medical catheter or a venipuncture needle. Our blood filtering approach is not intended to interrogate the total blood volume circulating through the targeted vein (Figure 1) since it would imply its total obstruction by the filter. In order to allow cell filtration, the blood flow should enter perpendicular to the holey membrane surface thus requiring a three-dimensional (3D) configuration. The 3D microdevice is composed by the microfilter which is integrated perpendicularly to a holding strip (Figure 1a). However, in order to characterize trapped

cells by conventional microscopy techniques, a planar positioning of the holey membrane is needed (Figure 1b). In order to combine these two orthogonal configurations within the same device, we propose a process to reversibly position the microfilter.

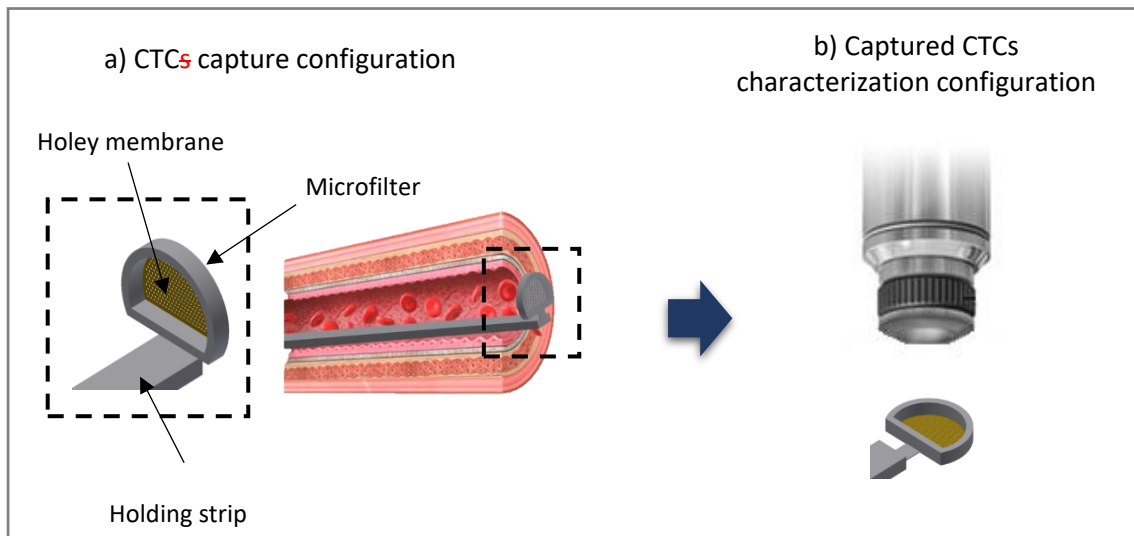


Figure 1: Configuration for CTC capture and characterization of the 3D microdevice. a CTC capture configuration with the microfilter integrated perpendicularly to the holding strip. b Captured CTCs characterization configuration with the holey membrane in a planar position.

### 3. From a planar fabrication technology to a three-dimensional configuration

Components involved in the whole 3D microdevice were fabricated using conventional microfabrication techniques prevalent in the microelectronic field. A planar cleanroom process was implemented to form the final 3D configuration in which microfilters were positioned perpendicular to the holding strip. The overall assembled device has to be stable enough to withstand *in vivo* experimental conditions, but at the same time, the assembly has to be reversible and the filter easy-to-handle in order to avoid the damage of captured cells.

Holding strips were designed to contain single or multiple (up to 6) microfilters. We investigated two strategies to integrate the microfilters to the holding strips and achieve the desired 3D configurations: a) a version allowing the mechanical insertion of the microfilters onto the holding strip and b) a foldable version where both pieces, the microfilter and the holding strip were fabricated as a single planar component.

#### 3.1. Mechanical insertion version

To implement this method, both microfilters and holding strips were engineered with complementary interlocking parts. This way the microfilter could be mounted on the designed slots of the holding strip before cell capture and then removed (Figure 2a). The part of the microfilter allowing stable insertion into the corresponding slot of the holding strip is termed as insertion tab. Designs were conceived to test the mechanical insertion through either a single insertion tab or double insertion tabs (Figure 2b).

### 3.2. Foldable version

In this strategy, the microfilter and the holding strip were fabricated as a single planar component. The link between both parts was designed as a tab allowing the microfilter to be folded at 90° with respect to the holding strip before cell capture and then folded back to its original position (Figure 2c). As proposed for the mechanical insertion version, designs with either one or two bending tabs were conceived for the foldable strategy (Figure 2d).

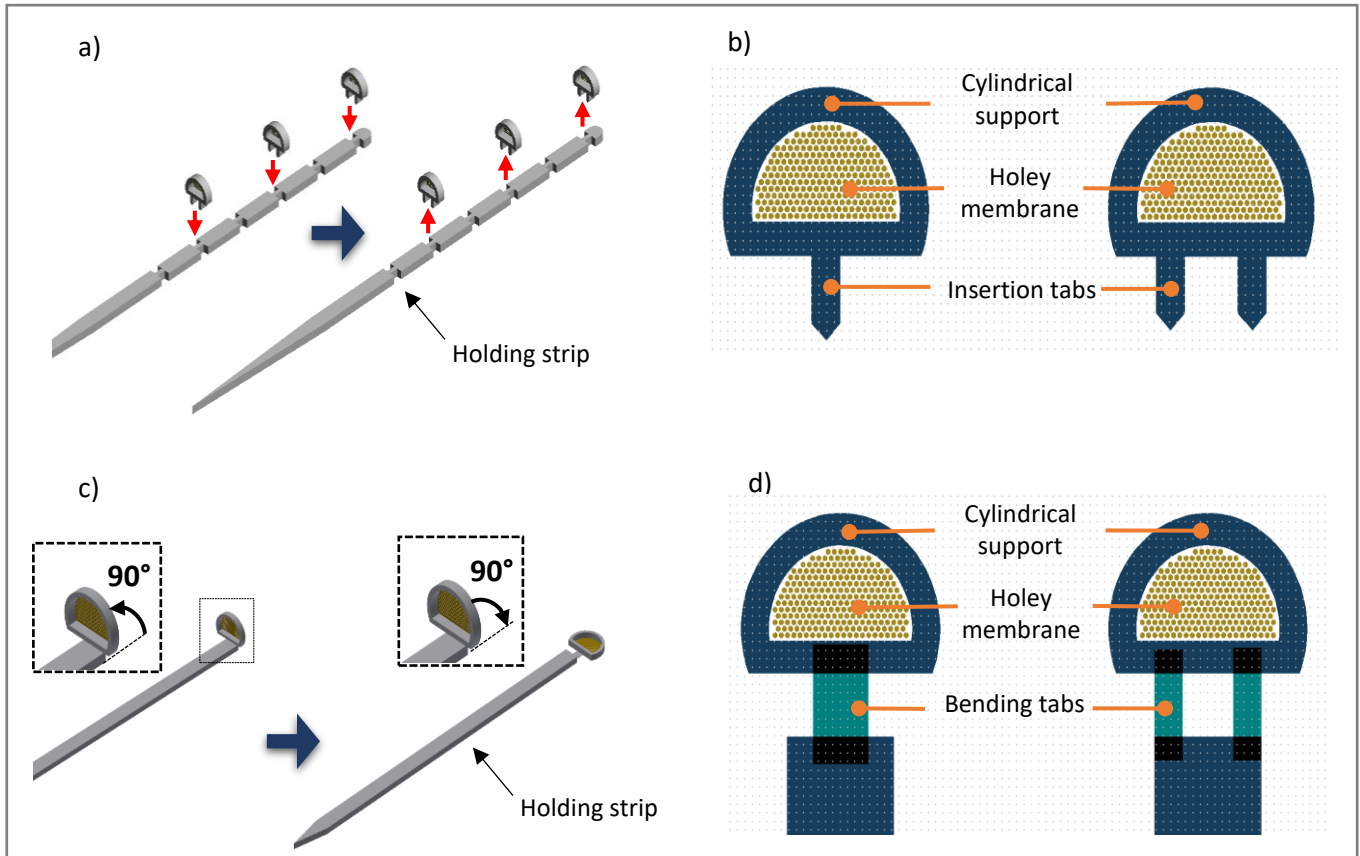


Figure 2: Strategies to form 3D microdevices. a Mechanical insertion of the microfilters into the holding strip slots and removal of the microfilters from the holding strip. b Schematic representation evidencing the single and double insertion tab versions. c Folding of the microfilter at 90° with respect to the holding strip and unbending of the microfilter. d Schematic representation evidencing the single and double bending tab version.

## 4. Design rules

The microdevice aims to perform *in vivo* CTC capture within the basilic vein, ranging from 2 to 7mm [11], one of the most common venipuncture sites. We thus envisioned inserting the microdevice using a peripheral venous catheter. Consequently, the overall geometrical dimensions of the device were constrained by the inner diameter of this medical consumable. We selected a 22G catheter size, corresponding to an inner diameter of 0.7mm, implying that the microdevice composed of the microfilter and the holding strip was designed to fit into the lumen of a 22G catheter (Figure 3a).

The geometry of the holey membrane was optimized to occupy the largest area of the lumen having a tolerance distance of  $60\mu\text{m}$ . In our prototypes we first fixed  $L_c$  at  $150\mu\text{m}$ . The width of the wall constitutive of the cylinder,  $t_c$ , was defined by technical constraints. Given photolithography process constraints we kept a  $L_c:t_c$  ratio equal to 2:1, thus  $t_c$  was set to  $75\mu\text{m}$  (Figure 3b). In addition, we aimed at fabricating the microdevice and the holding strip using the same batch process. For this purpose, the metal layer corresponding to the cylinder was grown in the same deposition step as the one grown for the holding strip implying that the thickness of the holding strip is equal to the length of the cylindrical structure  $L_c$ . The thickness of the metal layer corresponding to the holey membrane was set at  $5\mu\text{m}$  to minimize hydraulic resistance. Considering the targeted *in vivo* conditions of blood pressure and flow velocity, we chose the largest pore size reported for CTC isolation in clinical studies [12]. Thus, the size of the pores was set at  $12\mu\text{m}$  for all microfilter designs resulting in an arrangement of 247 pores across the holey membrane. The total length of the holding strip was set at 11mm. Regarding the mechanical insertion version, the distance between each device assembled along the holding strip was set at 2mm. The holding strip slots were designed with a margin of  $15\mu\text{m}$  with respect to the insertion tabs dimensions. Concerning the foldable version, two different tab lengths denoted as H, were tested ( $150\mu\text{m}$  and  $300\mu\text{m}$ ) and the thickness of the tab was fixed at  $10\mu\text{m}$  enabling bendability without rupture.

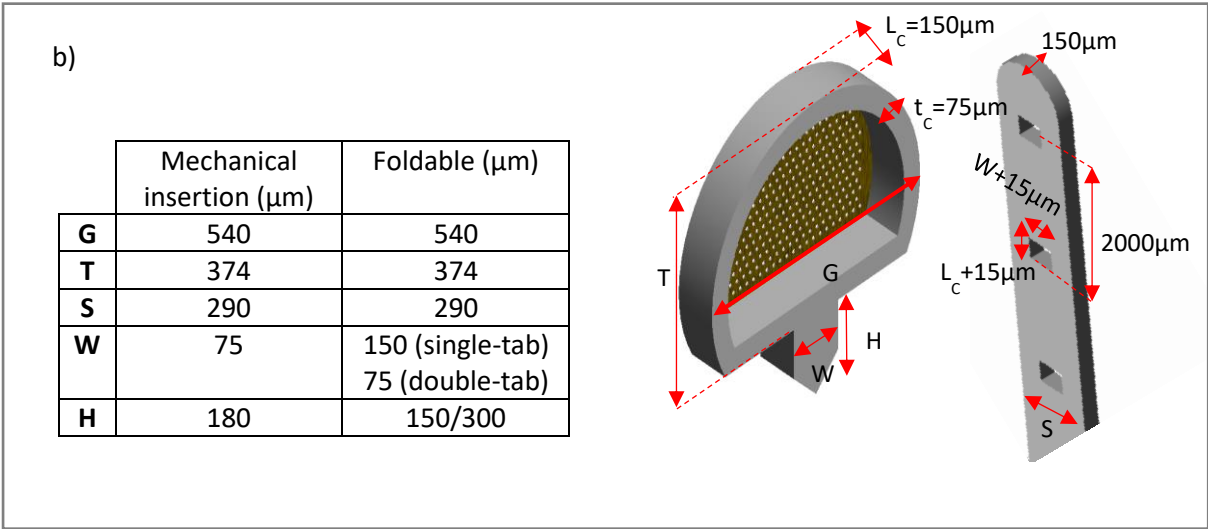
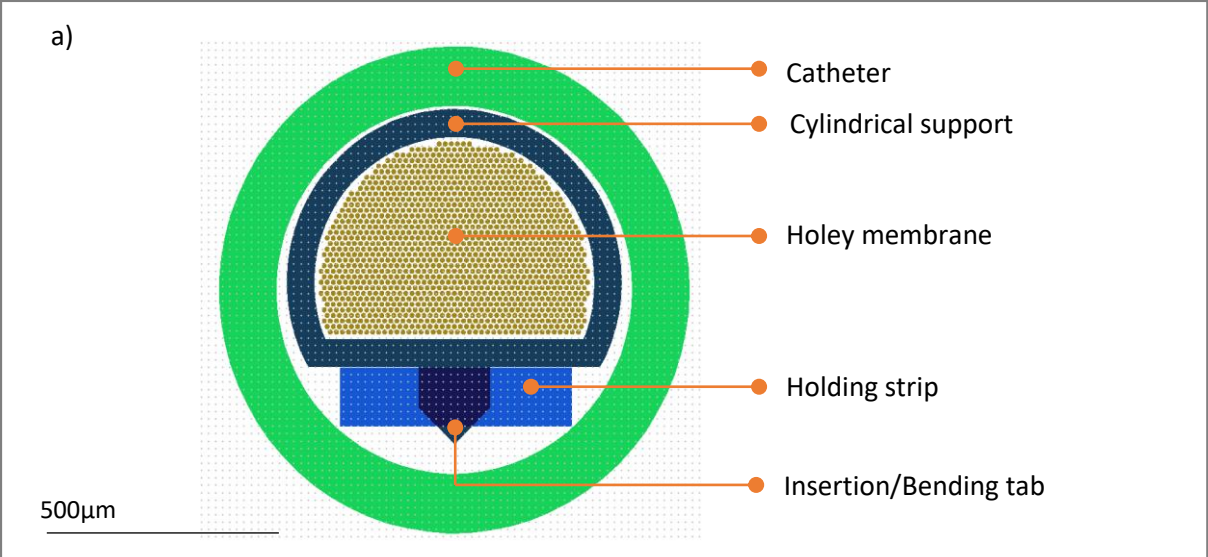


Figure 3: Overview of the design rules. a The microdevice and its holding strip fit into the available catheter lumen depicted in green, while maximizing the coverage area of the holey membrane. b Scheme depicting the overall dimensions of the microdevice and the holding strip.

## 5. Fabrication process

Among different available materials for electroplating, we selected Nickel as it has already been used for biomedical applications [13, 14]. All electrochemical depositions were performed using a RENA electroplating tool and NB SEMIPLATE NI 100 electrolytical bath (Microchemicals GmbH) at a current density of 5 and 20mA.cm<sup>-2</sup> for the 5 and 150µm thick layers respectively. In practice, microdevices were fabricated in a 5-step process, from which three steps correspond to UV photolithography and through-mask electrochemical deposition in a cleanroom environment (Figure 4).

A 4 inches Silicon wafer was cleaned using O<sub>2</sub> plasma (800W, 5min) and 50nm of titanium followed by 200nm of copper were subsequently deposited as seed layer. The first level (L1) defines the bendable tabs for the foldable design. It also includes labels in order to facilitate the identification of the microfabricated devices once detached from the substrate. A 10 µm-thick positive resist, AZ4562 (Microchemicals GmbH), was spin coated onto the wafer and then baked for 2min at 105°C. The resist was then exposed to a broadband UV light with an exposure dose of 230mJ/cm<sup>2</sup> (MA150 Mask Aligner, Karl Suss) and developed using MFCD26 (MicroChem Corp.) during 2min. A plasma cleaning step was performed to remove eventual non-polymerized resist residuals. The patterned wafer was then electroplated with a 10µm Nickel layer. Resist was then removed using acetone.

The second mask level (L2) corresponds to the microfilter holey membrane of the device for both the mechanical insertion and bending versions. Regarding the foldable design, a 20 µm-overlap between first and second levels was set to allow physical contact of the related metallic depositions. A plasma cleaning step was first performed (CF<sub>4</sub>+O<sub>2</sub>, 200W, 2min) to ensure both the removal of residuals of the photoresist used to define L1 layer, and a proper adhesion of the next photoresist layer. A 10µm layer of AZ4562 (Microchemicals GmbH) was spin-coated onto the wafer, exposed and developed in the same conditions as previously described. Subsequently, a 5µm-thick Nickel layer was electroplated and the remaining resist was then removed with acetone. The mean diameter of the pores obtained after the fabrication process was measured at  $D_p=11.88\pm 0.31\mu\text{m}$  which is very close to their nominal diameter of 12µm.

The third level (L3) is related to the microfilter hollow cylindrical structure and the holding strips. An overlap area of 30µm was designed between the second and third levels to ensure proper adhesion of the different parts of the device. For the bending version, an overlap was also defined to connect the bending tabs and the holding strip. As previously described, we performed a plasma cleaning step (CF<sub>4</sub>+O<sub>2</sub>). Two layers of dry film photoresist (WBR-2100, DuPont) were then laminated to obtain a 200µm-thick layer which was UV patterned with a 365nm UV light and 1100mJ/cm<sup>2</sup> exposure dose. The exposed photoresist was developed with Na<sub>2</sub>CO<sub>3</sub> solution heated to 28°C in an ultrasound bath (35kHz sweep mode) during 15min. A new plasma cleaning step (CF<sub>4</sub>+O<sub>2</sub>) was then carried out to ensure the removal of resist residues inhibiting the adhesion between electroplated Nickel layers L2 and L3 which could cause the detachment of the holey membrane. Then, a 150µm-thick layer of Nickel was electroplated and the remaining photoresist was removed with NF52 at 1% heated to 90°C. Finally, the silicon wafer was chemically etched using KOH solution, releasing the microfabricated pieces in solution. The seed layer was also removed, first using HF at 5% against Titanium and a mixture of 1% H<sub>2</sub>O<sub>2</sub> + 1% H<sub>2</sub>SO<sub>4</sub> + 98% H<sub>2</sub>O to chemically etch the Copper layer.

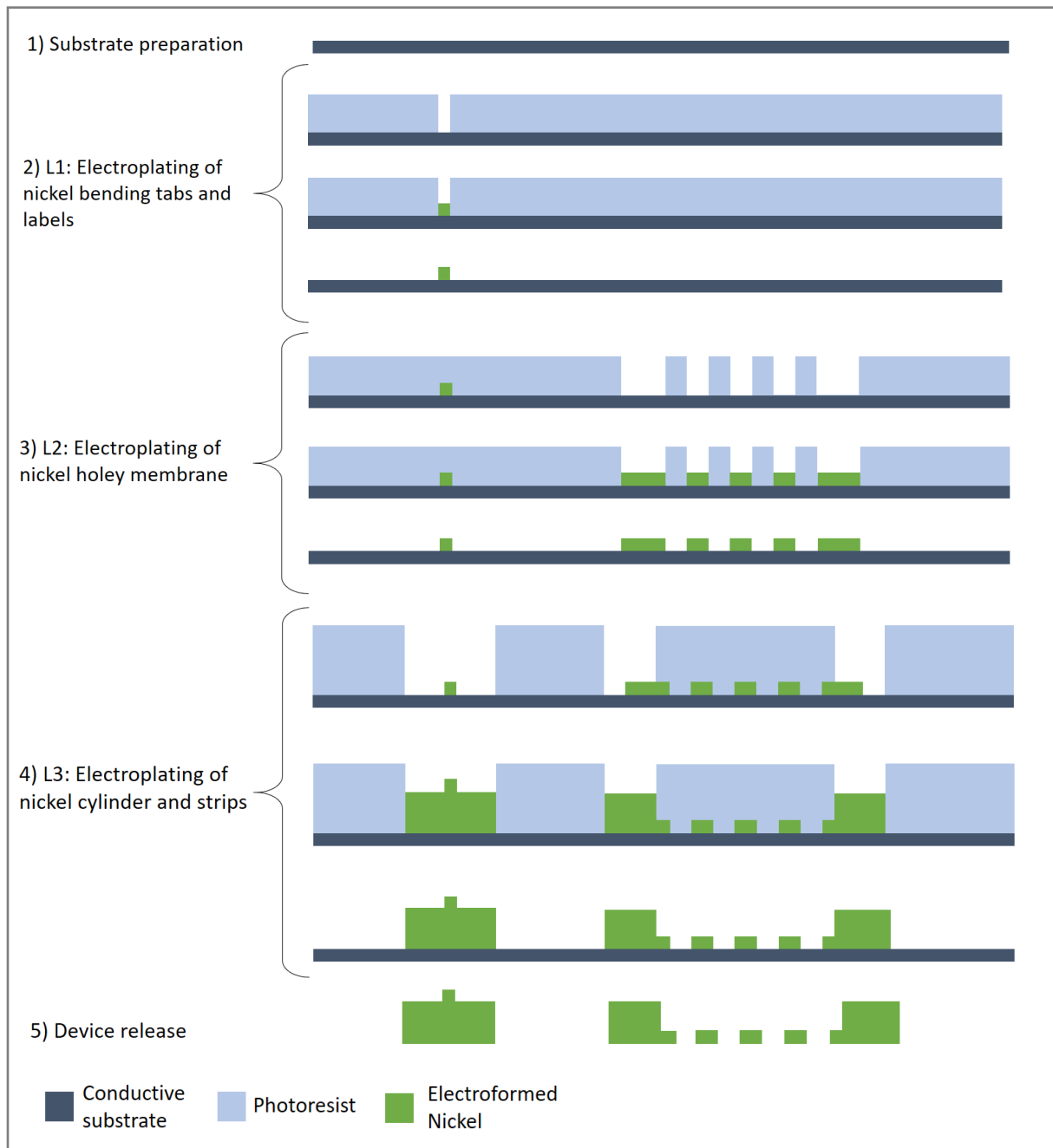


Figure 4: Schematic representation of the fabrication process. 1) A conductive layer is prepared on a silicon wafer. 2) A first photolithography process enables the deposition of Nickel bending tabs and labels by electroplating. 3) A second photolithography step is required to form the Nickel holey membrane by electroplating. 4) A third photolithography level allows the deposition of both the cylindrical structure and the holding strips. 5) A last process step is implemented in order to release devices from the conductive substrate.

## 6. Device integration

### 6.1. Microfilter integration

Two strategies were implemented to perform the perpendicular positioning of the microfilters onto the holding strips, and ensure self-centering and proper exposure to the flow. Regarding the mechanical insertion version, microfilters were first manually placed into a customized holder under optical inspection. The holder allowed keeping the insertion tabs pointing up (Figure 5a). In a second step, the slots of the holding strip were positioned to coincide with the insertion tabs. By applying a gentle pressure, microdevices and holding strips were mechanically locked. In order to ensure fastening, a droplet of biocompatible EP 630 glue (ratio 100:35) was deposited on the joint area, and cured at 80°C.

Regarding the foldable version, the microdevice was placed at the edge of a flat surface (Figure 5b) in order to have it suspended and allow free vertical access. Subsequently, under optical inspection and by means of tweezers, a gentle pressure was manually applied directly on the outer border of the device in order to fold the microfilter part at approximately 90°. The bending tab allowed to bend and unbend the microfilters one time without apparent fracture or damage. Further analysis will be required to determine the number of times this cycle can be performed before its rupture. Once placed at 90°, the microfilter kept a stable position in flow thanks to the stiffness of the bending tab.

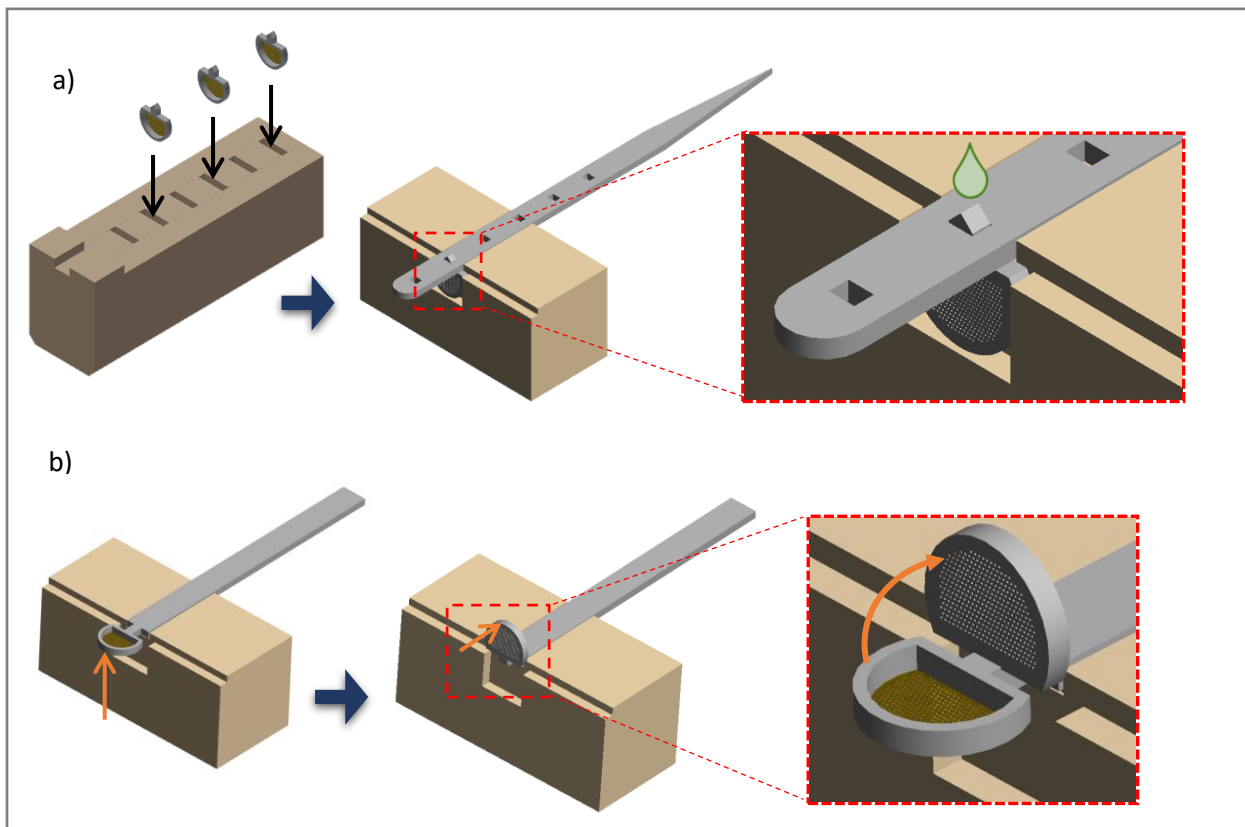


**Figure 5:** Schematic representation of the microfilter integration. **a** Manual mechanical insertion of the microfilters onto the holding strip. Inset depicts the mechanical locking of the microfilters into a holding strip slot and deposition of drop of glue to ensure fixation. **b** Manual folding of a single microfilter. Inset depicts the 90° folding of the microfilter with respect to the holding strip.

We were able to fabricate 3D microdevices with both mechanical insertion and foldable strategies. Both methods allowed us to integrate several microfilters on a single holding strip, Figure 6a and Figure 6b, potentially enabling the screening of larger amount of blood and thus increasing the overall

efficiency of the capture. Fluidic simulations (ANSYS Fluent® v15, see supplementary data Figure S1) show that a microfilter onto a holding strip induces an upstream and downstream flow perturbation. A stable and laminar flow is present at 1mm distance before and after the microdevice position on the holding strip. This was taken into account to define the 2mm interdistance between microdevices in series in order to recover a laminar flow at the entrance of each microdevice. This way, cells redistribute and reequilibrate leading to similar capture conditions for each one of the devices. The total number of captured cells is thus the addition of the captured cells per device resulting in an overall increase in cell capture efficiency. The three different Nickel deposition layers exhibited good adhesion, thus providing to the 3D microdevices enough robustness and stability to perform *in vitro* experiments. Regarding the mechanical insertion method, the glue step was delicate to implement. Controlling the size of the droplet was critical to avoid contamination of the holey membrane with the glue, as an example, glue residuals can be observed on the cylindrical structure of the microfilter in Figure 6a. Microfilters having a double insertion tab were easier to manipulate during their insertion into the holding strip slots and resulted in a better alignment with respect to the holding strip. Concerning the bending method, the 150 $\mu$ m bending tabs were preferred which resulted in a positioning of the microfilter just above the holding strip after bending. Similarly to the mechanical insertion method, the double-tab version resulted in a more precise alignment of the bent microfilter (Figure 6c). The mechanical properties of the 10 $\mu$ m Nickel layer constituting the tab allowed a proper bending and the stress generated during bending did not induce any apparent damage (Figure 6d).

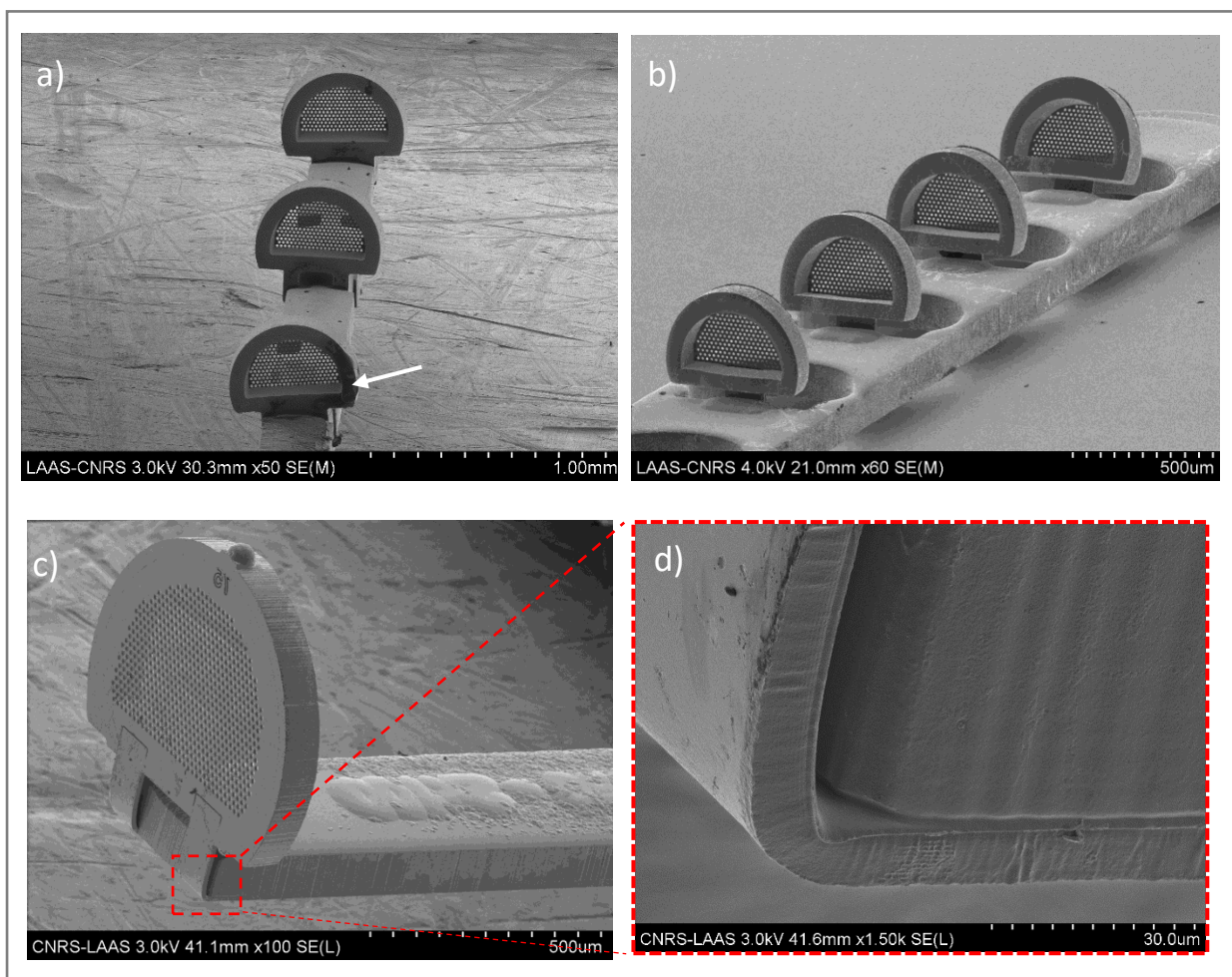


Figure 6: Scanning electron micrographs of assembled 3D microdevices. a Holding strip containing three double-tab microfilters integrated via the mechanical insertion strategy. White arrow points a

glue residual on the cylindrical structure. **b** Holding strip containing four single-tab microfilters integrated via the foldable strategy. **c** Holding strip containing one double-tab microfilter. **d** Magnification highlighting the folding of the bending tab.

In the same way as the assembly of the 3D microdevice, disassembly of the microfilters from their holding strip after cancer cell capture was performed manually. For both integration methods, the devices were placed on a flat surface and fixed using a piece of tape at the end of the holding strip. Under optical inspection and by means of tweezers, a gentle pressure was applied on the outer border of the microfilter in order to unfasten it from the holding strip or unbend it accordingly. This way, microfilters were positioned in a flat position with the holey membrane in contact using the substrate and ready to be characterized with conventional microscopy techniques.

## 6.2. Final Integration into an intravascular medical device

Our final objective is the integration of the 3D microdevice for its insertion within the vein through a conventional venous catheter. We propose a double-needle insertion system composed of a protection needle, an insertion needle and the 3D microdevice. The holding strip of our 3D microdevice is integrated to a 20G insertion needle. The Gauge system refers to the size of the needles and catheters for medical use. 18G and 20G needles present an inner diameter in the range of 0.790 - 1.041mm and 0.560 - 0.687mm respectively [15]. The end of the holding strip is glued in the 20G needle lumen in a way that both pieces maintain axial alignment. Then, the previously mentioned assembly is placed inside an 18G protection needle (Figure 8). This way, the overall microdevice-insertion needle ensemble is able to move freely through the 18G protective needle, allowing the microdevice to be inserted and retracted in the venous catheter. The whole set composed of the double-needle insertion and the microdevice is termed as intravascular device.

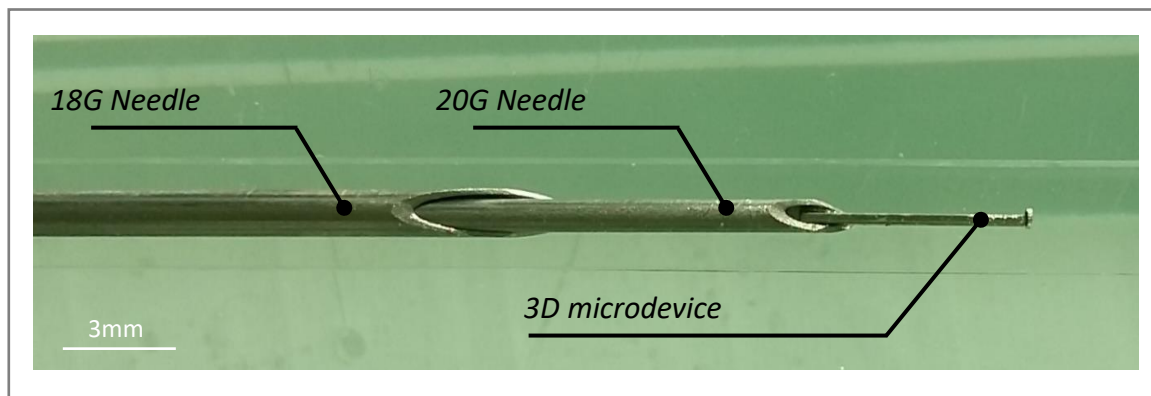


Figure 7: Image of the double-needle insertion system holding a 3D microdevice.

## 7. In vitro fluidic testing

### 7.1. Experimental conditions

As a first step to assess capture capability of the intravascular device containing the fabricated microdevice, a Polydimethylsiloxane (PDMS) fluidic platform was created. This PDMS fluidic chip aims at mimicking the venipuncture procedure. It was designed to contain a 3mm square cross-section channel corresponding to the vein where the capture is performed. A 1.3mm diameter lateral opening was conceived to allow the insertion of the intravascular device with the 3D microdevice in the retracted position as it would be performed in the lumen of a catheter. The 3D microdevice was then

exposed to the flow circulating across the channel with the holey membrane facing perpendicularly the incoming flow as it would be placed in the patient's vein. A peristaltic pump was used at 28 rpm to flow suspensions containing cancer cells through the fluidic chip obtaining a flow velocity of approximately 7.5cm/s which corresponds to the lower limit value of the real blood flow velocity found in a basilic vein as reported in literature [16]. This flow rate was used to perform all the subsequently described experiments. For those experiments we first used suspensions of cancer cells in cell culture medium, then cancer cells spiked into whole blood. Suspensions were flowed in the fluidic platform in close loop during 10 minutes. A rinsing step was systematically performed after capture with 40-45 mL of cell culture media in open loop keeping the same flow conditions. Cell fixation was performed using 500 $\mu$ L of formaldehyde solution at 4% (Formalin solution, 10% neutral buffered, SIGMA-ALDRICH®) introduced during 20min in the fluidic channel. Rinsing of the fixative solution was performed with 1mL of Dulbecco's phosphate-buffer saline (PBS) (Gibco). For experiments using suspensions of cancer cells in cell culture media, cells were dehydrated by flowing successively 25% v/v ethanol in PBS, 50% v/v ethanol in PBS, 75% v/v ethanol in PBS and ethanol solutions. For experiments involving cancer tumor cells spiked into whole blood, the dehydration process was not implemented to avoid bleaching of the fluorescence signal for fluorescence microscopy characterization of captured cells. In this case, devices with captured cells were let to dry at room temperature overnight before characterization.

Human prostate cancer cells (PC3) modified to express Green Fluorescent Protein (GFP) were used as our model to conduct experiments. Roswell Park Memorial Institute (RPMI) medium is used in cell biology for culture mammalian cells. Our cells were cultured in RPMI medium 1640 (1X) + GlutMAX™-I + 25mM HEPES (Gibco), supplemented with 10% fetal bovine serum (Gibco), 1% penicillin/streptomycin (Gibco), and 1% Geneticin® (Gibco). Cell culture dishes (CORNING Flask) were incubated at 37° in a humidified atmosphere containing 5% of carbon dioxide. Cells grown to confluence were rinsed with Dulbecco's phosphate-buffer saline (Gibco) and collected in RPMI medium following detachment using Trypsin-EDTA (1X) (Gibco). Cell suspension was then diluted to obtain the expected concentrations and added to 40mL of RPMI medium. Blood from healthy donors was collected in Ethylene Diamine Tetra Acetic acid (EDTA) tubes in order to perform capture experiments with whole blood. Here, 1mL of RPMI containing the adequate number of PC3-GFP cells in order to reach the expected final concentration was spiked into 24mL of whole blood. Concentrations used ranged from 5000 to 100 cells per mL of RPMI medium or blood. We stained the nucleus of the cells with a nucleic acid stain, Hoechst (350 and 461nm excitation and emission wavelengths respectively). Using GFP and Hoechst emission signals, we were able to identify the isolated cells after capture. To double-check and confirm first observations, a second characterization was performed using a scanning electron microscope (SEM Hitachi S-4800) after metallization of the filter. The correlation of both characterization techniques enabled to confirm the exact number of cells trapped in the filter.

## **7.2. Cancer cell capture in culture media**

Presence of PC3-GFP cells onto the holey membrane of the tested microfilters, [Figure 8](#), confirmed the capture capability of the microdevice for concentrations ranging from 5000 to 100 cells per mL. We can notice that cells adhere to the holey membrane surface after physical capture. Considering the protrusions formed by the cells on the holey membrane ([Figure 8b](#)) the Nickel microfilter can be considered as conducive to cell adhesion. It has been reported that cell adhesion is favored on substrates presenting a roughness at the nanoscale [17]. The surface roughness obtained with the electroplating technique was measured at 20nm on the holey membranes of the microdevices. This adherence of cells on the holey membrane after capture is important for cells to withstand subsequent rinsing steps and allow further analysis of trapped cells. It turned out that captured cells remained attached to the surface of the holey membrane during subsequent removal from the fluidic channel, cell fixation, and characterization indicating an overall robust adhesion at the microfilter surface.

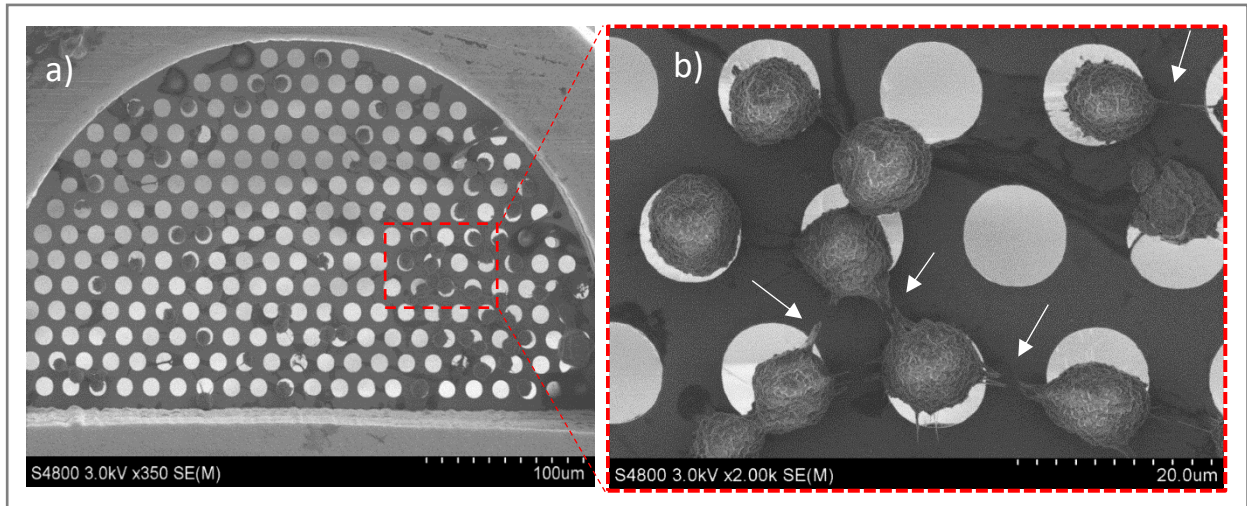


**Figure 8:** Scanning electron micrographs of a foldable microfilter after cell capture in culture medium at a concentration of 5000 cells per mL and a capture time of 10 minutes. **a** Overall view of the filter, captured cells are observed in some pores all over the holey membrane area. **b** Magnification on trapped cells. White arrows point some examples of the observed cell protrusions.

For a cell concentration of 5000 cells per mL, the number of captured cells was  $C_c=60$  within 10 minutes. For cells in suspension at a lower concentration, 1000 cell per milliliter, the average number of captured cells was  $C_c=11.2 \pm 6.38$  (mean  $\pm$ SD,  $n=5$ ). For these enumerations we only considered cells expressing GFP and Hoechst stained, and further identified by SEM. Cells were also isolated from a suspension at 100 cells per mL with an average number of  $C_c=6 \pm 1.73$  ( $n=3$ ).

The size distribution of the cell suspension used to perform experiments was measured using a cell counter device (Scepter™, Merck Millipore) providing a mean cell diameter of approximately  $19 \pm 2 \mu\text{m}$ . It can be noticed in Figure 8 that cells are smaller than the pore diameter after capture. This is due to fixation and dehydration processes conducted before electron imaging which reduces cell size of about 50%.

### 7.3. Cancer cell capture in blood

Blood is considered as a complex fluid due to its heterogeneity and rheological properties. These blood characteristics could influence the cell capture performance of the microdevice. Before evaluating cell capture, we first assessed the degree of contamination within the holey membrane when processing whole blood samples with no cancer cells. No clogging of the holey membrane pores was noticed after whole blood exposure during 10 minutes. We mostly identified platelets adhering to the holey membrane surface and very occasionally some blood cells probably corresponding to white blood cells (see supplementary data Figure S2).

In a second set of experiments, the capture performance of the microdevices was evaluated from suspensions consisting of spiked PC3-GFP cells into whole blood. Figure 9 correlates SEM with fluorescence images evidencing captured PC3-GFP cells onto the holey membrane. Contamination level is relatively low and cells exhibit a similar morphology as those captured from culture medium samples (Figure 9a). Remarkably, no clogging of the holey membrane was observed.

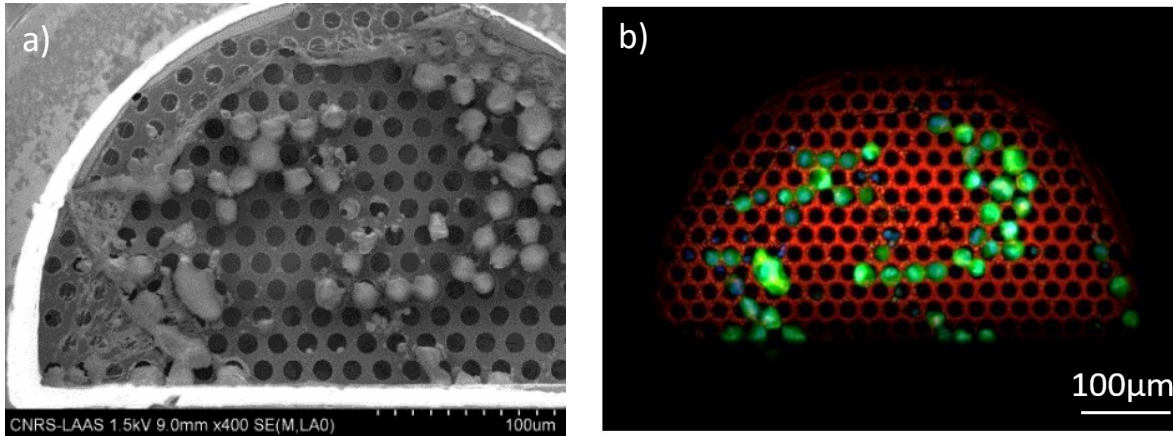


Figure 9: Correlation between SEM and fluorescence images of a device assembled using the mechanical insertion strategy. The concentration was 10000 cells per mL of blood. a SEM micrograph. A thin unidentified layer is present at the contour of the holey membrane, however pores are not clogged. b Corresponding fluorescence image.

For a cell concentration of 10000 cells per mL of blood, the number of captured cells was approximately  $C_c=50$  within 10 minutes. Using a cell concentration of 1000 PC3 cells, a mean value of  $C_c=2.83 \pm 2.45$  ( $n=5$ ) was measured.

Unlike conventional microfiltration techniques involving an obstructive filter screening the entire blood volume, our microfilter area just represents 0,7% of the fluidic chamber cross section. The size of our microdevices was designed to meet medical requirements and avoid any risk of thrombosis foreseeing a future use *in vivo*. Fluidic simulations show that, when exposed to a laminar flow, the microfilter induces a perturbation and part of the fluid flows around the microfilter. The presence of the holding strip at the microfilter vicinity also increases hydrodynamic resistance resulting in a reduced final volume passing through the holey membrane. As cells are captured on the holey membrane, the hydrodynamic resistance of the microdevice increases and a drop in the effective flowrate passing through the filter appears. At a threshold of the number of blocked pores by captured cells, some recirculation flow is induced and the flow does pass through the filter anymore. The capture efficiency reported here is therefore peculiar to the design of the microdevices and the number of pores contained in the holey membrane. PC3 capture from whole blood at cell concentrations lower than 1000 PC3 cell per mL were tested but those experiments did not reveal any capture of cancer cells. We believe that multiplying the number of microfilters onto the same strip, longer exposures to the flow, as well as improvements in microdevice design would enable the increase of captured cells fraction. Inserting our microdevices into a patient forearm vein through a catheter is a minimally invasive technique to access blood and could be repeated frequently enabling precise monitoring of pathology evolution.

## 8. Conclusions

We proposed an innovative 3D microdevice for the *in vivo* capture of cancer cells based on their specific physical characteristics. A cleanroom process was developed to fabricate components of the microdevice implementing standard planar microfabrication technologies. Two different assembly strategies were investigated to assemble the microfilter and holding strip constituting the final 3D microdevice. Microdevices were designed to be compatible with medical consumables involved in standard venipuncture procedures, foreseeing their use in clinical routine. Devices were also adapted to conventional characterization workflows. The prototype was validated *in vitro* using a fluidic

platform mimicking *in vivo* conditions of blood pressure and flow velocity. We succeeded in capturing human prostate cancer cells (PC3) spiked into whole blood in a few minutes, with no blood preprocessing required and with low contamination levels.

## Acknowledgements

This work was supported by the French National Research Agency (ANR-15-CE19-0020). This work benefited from the LAAS-CNRS micro and nanotechnology clean room facility, member of the French RENATECH network.

## References

- [1] Cohen, S. J. *et al.* Relationship of Circulating Tumor Cells to Tumor Response, Progression-Free Survival, and Overall Survival in Patients With Metastatic Colorectal Cancer. *Journal of Clinical Oncology* **26**, 3213–3221 (2008).
- [2] de Bono, J. S. *et al.* Circulating Tumor Cells Predict Survival Benefit from Treatment in Metastatic Castration-Resistant Prostate Cancer. *Clinical Cancer Research* **14**, 6302–6309 (2008).
- [3] Harouaka, R. A., Nisic, M. & Zheng, S.-Y. Circulating tumor cell enrichment based on physical properties. *Journal of laboratory automation* **18**, 455–468 (2013).
- [4] Seal, S. H. A sieve for the isolation of cancer cells and other large cells from the blood. *Cancer* **17**, 637–642 (1964).
- [5] Ferreira, M. M., Ramani, V. C. & Jeffrey, S. S. Circulating tumor cell technologies. *Molecular Oncology* **10**, 374–394 (2016).
- [6] Cima, I. *et al.* Label-free isolation of circulating tumor cells in microfluidic devices: Current research and perspectives. *Biomicrofluidics* **7**, 011810 (2013).
- [7] Saucedo-Zeni, N. *et al.* A novel method for the *in vivo* isolation of circulating tumor cells from peripheral blood of cancer patients using a functionalized and structured medical wire. *International Journal of Oncology* (2012).
- [8] Vona, G. *et al.* Isolation by Size of Epithelial Tumor Cells. *The American Journal of Pathology* **156**, 57–63 (2000).
- [9] Ntouroupi, T. G. *et al.* Detection of circulating tumour cells in peripheral blood with an automated scanning fluorescence microscope. *British Journal of Cancer* **99**, 789–795 (2008).
- [10] Adams, D. L. *et al.* The systematic study of circulating tumor cell isolation using lithographic microfilters. *RSC Adv.* **4**, 4334–4342 (2014).
- [11] Purvis, E. S., Hyde, G. L. & Peck, D. Anatomy of arm veins: Significance for vein valve transplantation. *Clinical Anatomy: The Official Journal of the American Association of Clinical Anatomists and the British Association of Clinical Anatomists* **5**, 45–49 (1992).
- [2] Khetani, S., Mohammadi, M. & Nezhad, A. S. Filter-based isolation, enrichment, and characterization of circulating tumor cells: KHETANI *et al.* *Biotechnology and Bioengineering* **115**, 2504–2529 (2018).
- [13] Sonofuchi, K. *et al.* Quantitative *in vivo* biocompatibility of new ultralow-nickel cobalt-chromium-molybdenum alloys: NEW ULTRALOW-Ni Co-Cr-Mo ALLOY BIOCOMPATIBILITY. *Journal of Orthopaedic Research* **34**, 1505–1513 (2016).
- [14] Sevcikova, J. & Pavkova Goldbergova, M. Biocompatibility of NiTi alloys in the cell behaviour. *BioMetals* **30**, 163–169 (2017).
- [15] Ahn, W., Bahk, J.-H. & Lim, Y.-J. The “gauge” system for the medical use. *Anesthesia & Analgesia* **95**, 1125 (2002).
- [16] Ooue, A. *et al.* Changes in blood flow in a conduit artery and superficial vein of the upper arm during passive heating in humans. *European Journal of Applied Physiology* **101**, 97–103 (2007).
- [17] Chen, W. *et al.* Nanoroughened Surfaces for Efficient Capture of Circulating Tumor Cells without Using Capture Antibodies. *ACS Nano* **7**, 566–575 (2013).